

Two-Finger Soft Gripper Force Modulation via Kinesthetic Feedback

Stephanie O. Herrera, Tae Myung Huh, Dejan Milutinović

Abstract—We investigate a method to modulate contact forces between the soft fingers of a two-finger gripper and an object, without relying on tactile sensors. This work is a follow-up to our previous results on contact detection. Here, our hypothesis is that once the contact between a finger and an object is detected, a controller that keeps a desired difference between the finger bending measurement and its bending at the moment of contact is sufficient to maintain and modulate the contact force. This approach can be simultaneously applied to both fingers while getting in contact with a single object. We successfully tested the hypothesis, and characterized the contact and peak pull-out force magnitude vs. the desired difference expressed by a multiplicative factor. All of the results are performed on a real physical device.

I. INTRODUCTION

Soft robotic grippers hold significant potential for tasks beyond simple pick-and-place operations, enabling more sophisticated dexterous manipulation. While demonstrations and models of such manipulation have been presented in the literature [1]–[3], most do not incorporate contact force measurements or force modulation, relying instead on the inherent compliance of the gripper in open-loop systems. However, to achieve more advanced functions, such as in-hand manipulation in unstructured environments with unknown object properties, it becomes essential to understand and control the forces involved, enhancing precision and effectiveness.

Tactile sensors, even in soft grippers, have been the primary method for detecting contact and measuring contact forces [4]–[6]. Although tactile sensors provide direct force measurements, their effectiveness can be limited by the complexity of integration and the wear and tear of contact surfaces over time, which may compromise consistent and reliable sensing.

Motivated by these limitations, we propose a feedback control-based kinesthetic sensing approach for soft grippers, where contact events are detected by monitoring changes in the reference tracking error, as demonstrated in our previous work [8]–[11]. Kinesthetic sensing in humans refers to the awareness of body movement and sensory feedback from receptors within muscles, tendons, and joints [12]. Similarly, bending sensors—either embedded within the gripper fingers or used remotely—can detect interaction forces by comparing desired finger bending with actual bending measurements. In our earlier studies, we explored this kinesthetic sense of touch using a single robotic soft-finger embedded with a resistive bending sensor, successfully detecting contact

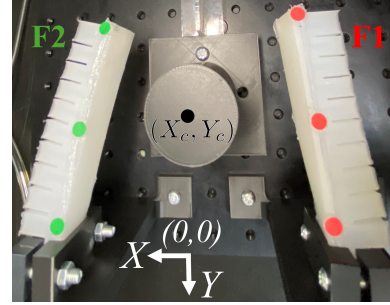


Fig. 1. Two-finger soft gripper experiment setup: Fingers F1 and F2 are actuated by feedback control using their bending measurements and outputting a control variable for the corresponding finger inflation pressure. The cylindrical object positioned at (X_c, Y_c) is mounted on a force sensor which we use to measure contact forces depicted along the X and Y directions. The finger design is based on [7].

between the finger and an object [11] by identifying the moment when the curvature reference tracking error increased due to contact force with the object. Recently published work [13], based on fluidic input sensing (rather than bending), has also demonstrated similar contact detection between a soft finger and the environment. However, these approaches have yet to modulate the contact force during interaction.

Following up on our previous work, we adopt here the previously used reference tracking feedback controller structure and design the procedure from [8] to investigate the use of feedback control to modulate contact forces between two soft fingers and an object. Therefore, our paper contributions are:

- validation of the reference tracking controller from [8] in our setup with different soft fingers and bending measurements;
- feedback control for modulating contact forces between soft fingers and an object using only soft finger bending measurements;
- characterization of the feedback control-enabled contact and peak pull-out forces between two soft fingers and an object.

This paper is organized as follows. Section II outlines the problem statement concerning the modulation of contact forces. In Section III, we present preliminary findings of the bending reference tracking controller, which are part of our validation of the reference tracking controller. Section IV describes the force-modulating controller and its design. Section V reports characterization experiments, and Section VI provides conclusions based on our results.

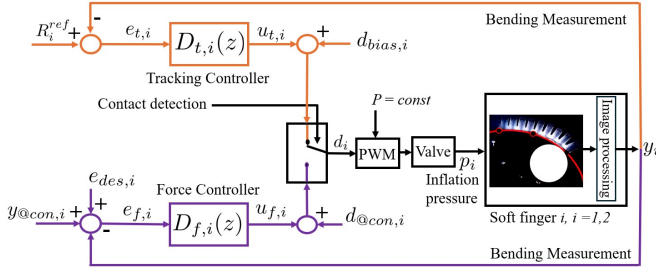


Fig. 2. The soft finger feedback control: R_i^{ref} is the bending reference for the bending measurement y_i of the control loop with the tracking controller $D_{t,i}(z)$ (orange). The contact detection, which is based on magnitudes of $e_{t,i}$ and d_i , switches to the force modulating control with the controller $D_{f,i}(z)$ (purple). The signals $y_{@con,i}$ and $d_{@con,i}$ are bending and duty cycle at the time of contact, $d_{bias,i}$ compensates for the dead zone in actuation, and P depicts the constant air pressure source.

II. PROBLEM FORMULATION

Figure 2 depicts two feedback control loops for the control of a single finger in Fig. 1. One of the loops includes the controller $D_{t,i}(z)$ and the other the controller $D_{f,i}(z)$. Both controllers use the same bending-related measurement y_i and output a duty cycle d_i , which dictates the finger inflation pressure p_i . At any time, only one of the feedback control loops is active.

The controller $D_{t,i}(z)$ is part of the *reference tracking* control loop which enables contact detection between the finger and an object. The controller was designed and demonstrated in [11] using resistive bending sensitive sensors mounted onto the dorsal side of the finger. In [11], it was stated that the controller design process could be applied to other types of bending-sensitive sensors and measurements. Therefore, our first problem (P1) is to validate the use of the reference tracking controller on the two-finger gripper in Fig. 1.

After contact is detected, there is a switch from the reference tracking control to *force modulation control* with the controller $D_{f,i}(z)$. We propose to design the controller $D_{f,i}(z)$ that, for the desired error value $e_{des,i} = 0$, results in the controller input $e_{f,i}$ convergence to 0, and the bending measurement y_i convergence to the value of the bending measurement at the moment of contact detection $y_{@con,i}$. Under these conditions, the contact of the finger with an object is a gentle or light one [11].

We hypothesize that if we set $e_{des,i} > 0$, it will induce an increase in the inflation pressure, i.e., the finger bending further and a larger contact force. Therefore, our second problem (P2) is to test the hypothesis about force modulation using $e_{des,i}$ and the controller $D_{f,i}(z)$.

Due to the elasticity of the soft finger body, we expect that the relation between $e_{des,i}$ and the contact force is linear, or at least monotonously increasing and similar for both fingers. For this reason, our goal here (P3) is to characterize the relation between $e_{des,i}$ vs. contact forces and two-finger pull-out forces.

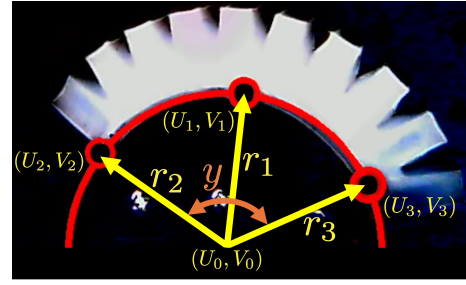


Fig. 3. Bending measurements y : (U_k, V_k) , $k = 1, 2, 3$ are pixel coordinates of the centers of the circular markers, (U_0, V_0) is the center of a circle fitted to the three markers. Vector magnitudes $|r_k|$, $k = 1, 2, 3$ are identically equal.

III. TECHNICAL PRELIMINARIES - REFERENCE TRACKING CONTROLLER AND CONTACT DETECTION

Both feedback control loops depicted in Fig. 2 depend on the finger-related bending measurement. The measurement is computed from the camera video frame-detected color markers as shown in Fig. 3. The figure also shows that frame-detected markers are not labeled in any particular order, which is a consequence of using OpenCV functions. For this reason, the bending y is computed as

$$y = \max_{k,j,k \neq j} \left\{ \arccos \frac{r_k^T r_j}{|r_k| |r_j|} \right\}, \quad k, j = 1, 2, 3, \quad (1)$$

where $r_k = [U_k - U_0, V_k - V_0]^T$, which is a column corresponding to the vector r_k from Fig. 3 which starts at (U_0, V_0) and ends at (U_k, V_k) pixel coordinates. $|r_k|$ is the vector magnitude and the superscript T denotes a matrix transpose. In the sequel, we use y_i , $i = 1, 2$ for the bending y measurement computed for each finger and express it in degrees.

Reference Tracking Controller: Here, we follow a process of the controller design as described in [11]. In this process, we use a pseudo-random sequence of duty cycles (d) and the corresponding bending measurements (y), both sampled with a sample time of $T_s = 0.01$ sec. Using system identification, we estimate a 2nd order ARX model (AutoRegressive with eXogenous inputs model) from d to y , which has a z-domain form

$$A(z)y(z) = B(z)d(z) + e_m(z), \quad (2)$$

where $y(z)$, $d(z)$ and $e_m(z)$ are z-domain images of the output, input and modeling errors, and $A(z)$ and $B(z)$ are polynomials

$$\begin{aligned} A(z) &= z^2 + a_1z + a_2 = z^2 - 0.7655z + 0.03624, \\ B(z) &= b_1z + b_2 = 0.04074z + 0.3601. \end{aligned} \quad (3)$$

This yields that the z-domain transfer function $G(z)$ of the soft finger is

$$G(z) = \frac{B(z)}{A(z)}. \quad (4)$$

The analysis in [11] shows that the ramp-signal tracking error $e_{t,i}$ convergence to 0, i.e., zero-error tracking of a ramp

reference, can be achieved with a controller that has the following z-domain transfer function

$$D_{t,i}(z) = K_t \frac{z - z_t}{(z - 1)^2}. \quad (2)$$

We used the discrete-time root locus analysis in MATLAB's `rtool` to tune the controller $D_{t,i}(z)$ parameter values to $z_t = 0.97$ and $K_t = 0.066$.

The use of the tuned feedback controller is illustrated by the experimental results in Fig. 4. Figure 4A shows bending measurement data for both fingers (red and blue lines) when the triangular reference signals (green and magenta lines), slightly shifted in time, were used as reference signals for the feedback control of the fingers in Fig. 1. In the experiment, both fingers were free to move without any contact among them or with another object. As a result of the reference tracking, the fingers periodically flexed and extended. The tracking errors $e_{t,i}$ are largest after the change in reference slopes, which creates error jumps as seen in Fig. 4B. The same plot also shows that during the periods of positive or negative slopes, the measurements converge to the corresponding references. This behavior is expected since the controller $D_{t,i}(z)$ is designed as a ramp reference tracking controller.

Figure 4B also shows the type of data used to estimate the empirical cumulative distribution functions (CDFs) of the tracking error for both fingers. We found that 80% of recorded errors are below $e_{tr,1} = 3.88$ and $e_{tr,2} = 4.71$ for Finger 1 and Finger 2, respectively. We use these values as threshold values for contact detection since the largest errors appear when the slope of the reference changes. However, the reference signal slope change will never happen during the grasping of an object since the fingers are going to be in contact with the object during the first positive slope of the reference.

Figure 4C shows the output of the controller $d_i = u_{t,i} +$

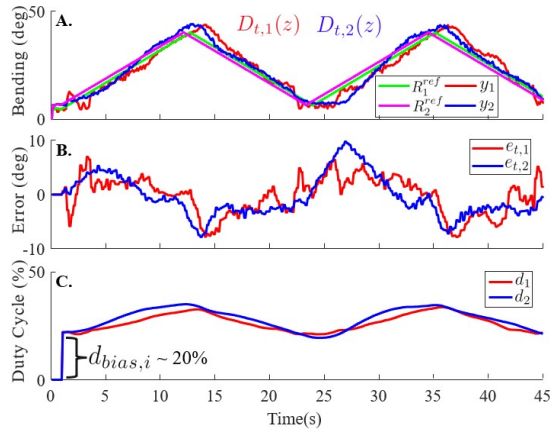


Fig. 4. Bending reference tracking: (A) Triangular reference inputs R_1^{ref} (green) for Finger 1 (F1) and R_2^{ref} (magenta) for Finger 2 (F2). The bending measurements y_1 (red) for F1 and y_2 (blue) for F2. (B) The tracking errors $e_{t,1}$ (red) for F1 and $e_{t,2}$ (blue) for F2. (C) The duty cycle d_1 (red) for F1 and d_2 (blue) for F2 control outputs. During our experiments, we found that a dead zone of control action was approximately 20%.

$d_{bias,i}$, which is the duty cycle that produces the inflation pressure p_i from the constant input pressure source P . In the process of tuning the controller, we found that the valve through which we generated p_i had a dead zone of about 20% of the duty cycle, which is the value $d_{bias,i}$ added to the controller $D_{t,i}(z)$ output.

Contact Detection: Figure 4 shows the plots corresponding to freely moving soft-fingers. However, if the motion of the fingers is impeded by contact with an object, the reference tracking error increases while the duty cycle is well above the dead zone duty cycle of 20%. At the time point indicated by the red (blue) dashed line in Fig. 5, the duty cycle is at 30% and Finger 1 (Finger 2) is above its error threshold $e_{tr,1}$ ($e_{tr,2}$), so we can conclude that Finger 1 (Finger 2) is in contact with the object. This triggers the switch from the tracking controller, $D_{t,i}(z)$, to the force controller, $D_{f,i}(z)$, for Finger 1 (Finger 2). While the contact detection can be further improved or formulated differently, it is not in the focus of our work here. The focus is on the method of force modulation after the contact detection when the controller $D_{f,i}(z)$ is active, which we discuss in the following section.

IV. FORCE MODULATION CONTROLLER

The role of the force modulating controller $D_{f,i}(z)$ in our approach is not only to maintain contact between the fingers and an object, but also to allow us to modulate the contact force. Since we memorize the bending measurement $y_{@con,1}$, $y_{@con,2}$ and the inflation pressure $p_{@con,1}$, $p_{@con,2}$ at the moment of contact, with $e_{des,i} = 0$ and using $D_{f,i}(z)$ providing the convergence of $e_{f,i}$ to 0, we can maintain the contact between the finger and an object with a minimal force (light-touch). A controller that provides this for the 2nd order model (2)-(3) has the form

$$D_{f,i}(z) = K_f \frac{z - z_f}{z - 1}, \quad (5)$$

where K_f is the controller gain, z_f is the real zero introduced by the controller and in our design the term $z - 1$ ensures the zero steady state error for tracking a step reference signal. The latter can be verified by evaluating $e_{f,i}(\infty) = \lim_{t \rightarrow \infty} e_{f,i}(t)$ using the finite value theorem in the z-domain as

$$e_{f,i}(\infty) = \lim_{z \rightarrow 1} (z - 1) \frac{1}{1 + D_{f,i}(z)} \frac{B(z)}{A(z)} \frac{zR}{z - 1} \quad (6)$$

$$= \lim_{z \rightarrow 1} \frac{R}{1 + K_f \frac{1 - z_f}{z - 1} \frac{b_1 + b_2}{1 + a_1 + a_2}} = 0, \quad (7)$$

where R is the magnitude of a step reference signal at $e_{des,i}$. Our hypothesis from P2 is that using the same controller $D_{f,i}(z)$ and $e_{des,i} > 0$, we can increase the contact force.

In all our experiments, the controller $D_{f,i}(z)$ has the parameters $K_f = 0.21$ and $z_f = 0.44$. We discuss the parameter K_f and z_f selection process after showing the results that our hypothesis from P2 is correct.

We first performed experiments with the force sensor-mounted cylindrical object from Fig. 1, which is positioned between the two fingers at (0, 15) cm. Consequently, we measured forces that the fingers applied to the object in

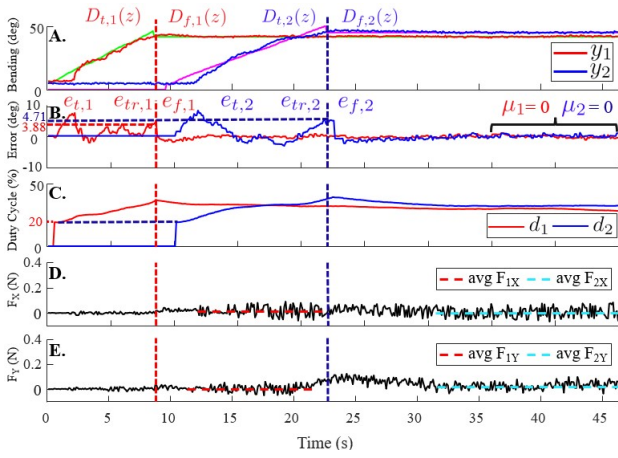


Fig. 5. Two-finger gentle force contact: (A) the solid green line is R_1^{ref} for the $D_{t,1}(z)$ controller and $y_{con,1}$ for the $D_{f,1}(z)$ controller. The solid magenta line is R_2^{ref} for the $D_{t,2}(z)$ controller and $y_{con,2}$ for the $D_{f,2}(z)$ controller. (B) Plots of controller tracking errors. The switch from $D_{t,1}(z)$ to $D_{f,1}(z)$ is when $e_{t,1} \geq e_{tr,1} = 3.88$ and the switch from $D_{t,2}(z)$ to $D_{f,2}(z)$ is when $e_{t,2} \geq e_{tr,2} = 4.71$. (C) Duty cycles d_1 (red) and d_2 (blue) for the inflation pressure of F_1 and F_2 , respectively. (D) and (E) are plots of X and Y force components for $e_{des,1} = e_{des,2} = 0$ on the cylindrical object of a radius $r = 2\text{cm}$ and positioned at the location $(X_c, Y_c) = (0, 15)\text{cm}$.

the X and Y directions and denoted them as F_X and F_Y , respectively. In our experiments, the force F_X is the difference between Finger 1 and Finger 2 forces on the object in the X direction while the force F_Y is a sum of Finger 1 and Finger 2 forces in the Y direction. The fingers were first controlled by their corresponding tracking controllers $D_{t,i}(z)$ with ramp references of the same slope that were initiated at different times (first Finger 1 and then Finger 2). Finger 1 was the first to get in contact with the object, switching from the $D_{t,i}(z)$ to $D_{f,i}(z)$ controller.

Light touch: The experiment results are plotted in Fig. 5. At the moment of Finger 1 contact detection, denoted as dashed red lines, we set $R_1^{ref} = y_{@con,1}$ and $e_{des,1} = 0$. After that time point (9 s), we see in Fig. 5B that the controller error $e_{f,1}$ is close to 0 and Fig. 5D and Fig. 5E show a gentle contact force of 0.006 N. At the moment of Finger 2 contact detection (23 s), denoted by dashed blue lines, we set $R_2^{ref} = y_{@con,2}$ and $e_{des,2} = 0$. Following this, we see in Fig. 5B that the corresponding error $e_{f,2}$ is also close to 0 and that the measured forces F_X and F_Y plotted in Fig. 5D and Fig. 5E are still small (0.03 N). This is all expected from the experiment with $e_{des,i} = 0$, $i = 1, 2$. The magnitude of the light touch forces as a function of $e_{des,i}$, including $e_{des,i} = 0$, is examined in Section V-A.

Force modulation controller: Fig. 6 shows the results from the same setup as in the light touch experiment. The only difference is that at the moment of Finger 1 contact detection, we set $R_1^{ref} = y_{@con,1}$ and $e_{des,1} = \mu_1 e_{tr,1} = 15.52$, where $\mu_1 = 4$ is a multiplicative factor. At the moment of Finger 2 contact detection, we set $R_2^{ref} = y_{@con,2}$ and $e_{des,2} = \mu_2 e_{tr,2} = 18.84$, using multiplicative factor $\mu_2 = \mu_1 = 4$. Now we can see in Fig. 6D that after the

Finger 1 contact, F_X has a shift in the value, which is well above the sensor noise level and after the Finger 2 contact is made, the force F_X value drops. Also, Fig. 6E shows that the force F_Y increases after both Finger 1 and Finger 2 contact detections, as expected.

In summary, the results illustrated in Fig. 5 and Fig. 6 confirm our hypothesis of being able to use the controller $D_{f,i}(z)$ to increase soft finger contact forces while maintaining the contacts, i.e., to modulate the contact force.

Controller parameters: The use of the controller $D_{f,i}(z)$ from (5) in the force modulating control loop results in the feedback loop gain

$$L(z) = K_f \frac{z - z_f}{z - 1} \frac{B(z)}{A(z)}. \quad (8)$$

We used the z -domain root locus from MATLAB's `rtool` and placed the zero $z_f = 0.44$ of the feedback loop gain $L(z)$ to obtain the root locus shown in Fig. 7. The root locus branches present paths along which the closed feedback loop poles move as $K_f > 0$ goes from 0 to ∞ . Our root locus has three branches. The first branch starts ($K_f = 0$) from a real pole at 0.05 and finishes ($K_f = \infty$) at $z_f = 0.44$. The other two branches start ($K_f = 0$) from poles at 0.71 and 1, and finish ($K_f = \infty$) in zero at -8.84 and infinity. In order to have a stable feedback control loop, we need to have all closed loop poles within the unit circle $|z| = 1$. For this reason, we need to take K_f before any of the three poles escapes the circle. After an initial selection of K_f in matlab and its reduction and fine tuning on the real system, we finally set $K_f = 0.21$.

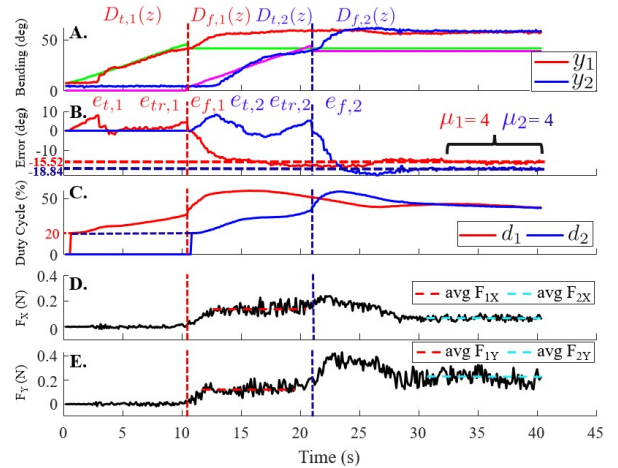


Fig. 6. Two-finger force modulation: (A) The solid green line is R_1^{ref} for the $D_{t,1}(z)$ controller and $y_{con,1}$ for the $D_{f,1}(z)$ controller. The solid magenta line is R_2^{ref} for the $D_{t,2}(z)$ controller and $y_{con,2}$ for the $D_{f,2}(z)$ controller. (B) Plots of controller tracking errors. The switch from $D_{t,1}(z)$ to $D_{f,1}(z)$ is when $e_{t,1} \geq e_{tr,1} = 3.88$ and the switch from $D_{t,2}(z)$ to $D_{f,2}(z)$ is when $e_{t,2} \geq e_{tr,2} = 4.71$. (C) Duty cycles d_1 (red) and d_2 (blue) for the inflation pressure of F_1 and F_2 , respectively. (D) and (E) are plots of X and Y force components for $e_{des,i} = \mu_i e_{tr,i}$, $\mu_i = 4$, $i = 1, 2$ on the cylindrical object of a radius $r = 2\text{cm}$ and positioned at the location $(X_c, Y_c) = (0, 15)\text{cm}$.

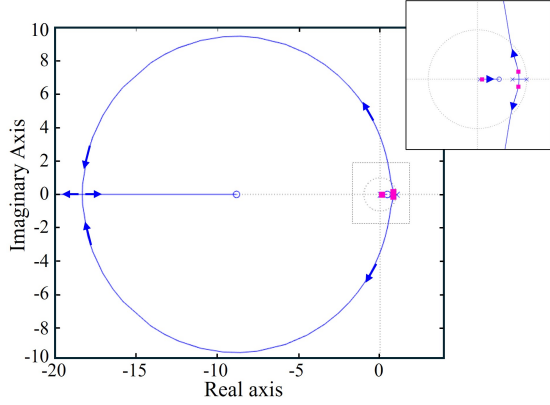


Fig. 7. The root locus for the force modulating controller $D_{f,i}(z)$ from (5). The root-locus branches are plotted in solid lines with the arrows indicating the branch directions as K_f goes from 0 to ∞ . The symbols 'o' and 'x' denote zeros and poles of the loop gain $L(z)$. The figure insert shows the part of the root locus framed by the dashed line, in which the blue circle represents the real zero $z_f = 0.44$. The magenta squares denote the poles for $K_f = 0.21$ and they are all inside the unit cycle, therefore, the closed loop system is stable.

V. EXPERIMENTS AND RESULTS

We first demonstrate the modulation of contact force using our kinesthetic feedback controller on a fixed object with a single finger. We then extend this capability to a two-finger grasp scenario, illustrating how force modulation can be applied on each finger when an unfixed object is misaligned with respect to the axis symmetry. Finally, we show how our controller adjusts contact forces to modulate pull-out forces.

Experiment Setup: We constructed two pneumatic soft fingers based on the design from the Soft Robotics Toolkit [14]. The gripper has a length of 107 mm, with the two fingers mounted 150 mm apart, facing each other in parallel. For bending measurements, we placed three marker stickers on each finger, spaced 27.3 mm apart, using two different colored stickers per finger.

We implemented our controller in Python on a PC, with a sampling time of 100 ms, matching the bending measurement rate from the marker tracking system. The RGB webcam (Logitech C210) was used in conjunction with a marker tracking library in OpenCV.

The air pressure for the grippers was supplied via a pressure control board, adapted from the design provided by the Soft Robotics Toolkit [14]. We modified the pressure source to use pressure-regulated wall-compressed air. The board controls the input pressure by adjusting the valve opening through PWM duty cycle, with a control frequency of 90 Hz.

For testing, we 3D-printed a cylindrical object (radius $r = 2$ cm, height = 8.4 cm) using PLA material. In the contact force modulation tests, we mounted the cylindrical object on a 6 DOF load cell (ATI, Gamma), which sampled data at 2.2 kHz and was fixed to an optical plate. For tests involving grasping an unfixed object, we placed the cylindrical object on an anodized optical plate, ensuring low friction (0.09).

For the pullout force tests, the load cell was mounted on a Franka Emika Research 3 robot arm. At the same time, the cylindrical object was attached to the load cell using cantilevered interconnects to prevent interference from the robot arm with the vision system. Once the two fingers grasped the cylinder object, the robot arm pulled it along the $-Y$ direction at a constant speed (-5 cm/s), measuring the real-time pull-out force.

A. Modulation of Contact Forces With Fixed Object

To test the contact force modulation of our controller (as shown in Fig. 6), we positioned the load cell-mounted cylinder at $(X_c = 0, Y_c = 15)$ cm. Fig. 8 shows the plot of Finger 1 (F1)'s contact force magnitudes vs. multiplicative factor μ_1 , where $e_{des,1} = \mu_1 e_{tr,1}$. We found using factor μ_i , $i = 1, 2$ useful to address the difference in the fingers. We expected to see a linear relation assuming that the soft finger in contact behaves as a loaded spring as described in the pseudo rigid body model [15]. We see that the plot shows the linear relation, although it also shows a slightly larger variation of forces as we applied larger μ_1 values.

B. Asymmetric Grasping of Unfixed Object

Fig. 9 depicts experiments in which the cylindrical object is positioned at $(X_c = 1.25, Y_c = 15)$ cm. Since $X_c \neq 0$, the left soft finger (F2) has to bend further until it reaches contact with the object.

At the beginning of the experiment, both fingers were controlled with ramp reference tracking controllers. The experiments started with $R_1^{ref} = 0$ and $R_2^{ref} = 0$ resulting in the configuration from Fig. 9A. Then we applied a ramp reference signal to R_1^{ref} , but keeping $R_2^{ref} = 0$ until the contact between (F1) and the object is detected (see Fig. 9B) when we switched from the tracking to the force modulating controller for (F1) with a constant $e_{des,1} = \mu_1 e_{tr,1}$ with $\mu_1 = 0$. After 10 sec, we applied a ramp reference signal to R_2^{ref} until the contact between (F2) and the object was

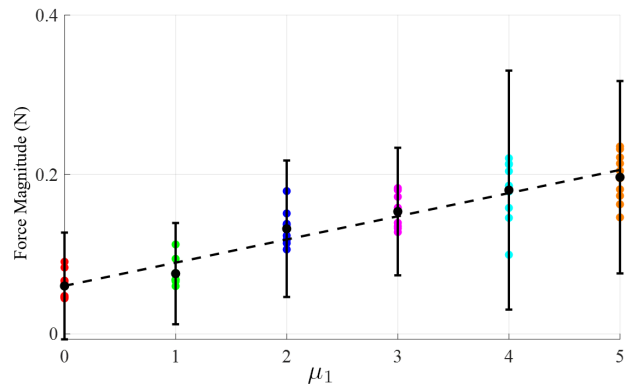


Fig. 8. Single finger force modulation: the normal force during contact, shown as colored circles, is plotted against the error values of the force controller for the cylinder with radius $r = 2$ cm and position at $(X_c, Y_c) = (0, 15)$ cm. The mean value for each configuration is shown as a solid black circle, and the best-fit line is depicted as a black dashed line. Gentle single-finger contact can be achieved by setting $e_{des,1} = 0$ for a resulting normal force of less than ~ 0.1 N. The maximum force achieved is ~ 0.25 N with $e_{des,1} = \mu_1 e_{tr,1} = 19.4$ when the multiplicative factor $\mu_1 = 5$.

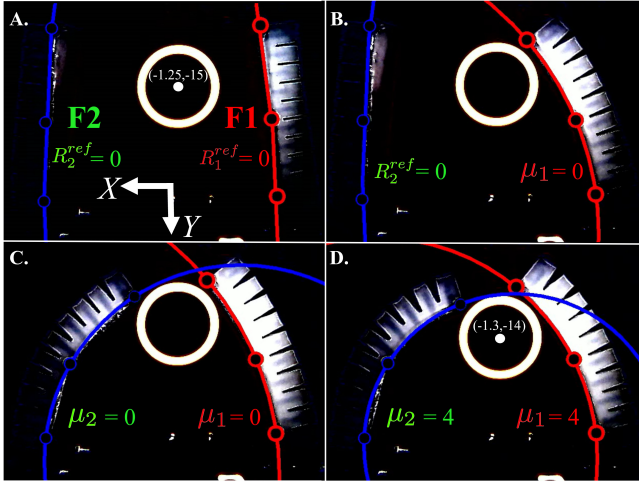


Fig. 9. Asymmetric grasping: (A) The free-floating cylinder is asymmetrically positioned between F1 and F2. (B) F1 makes contact with a small force ($\mu_1 = 0$) such that the cylinder remains stationary. (C) F2 makes gentle contact ($\mu_2 = 0$) while F1 remains in gentle contact ($\mu_1 = 0$) with the cylinder. (D) After the asymmetric gentle grasp is stabilized, the force controllers modulate contact forces ($\mu_1 = \mu_2 = 4$) such that the cylinder moves slightly to the right and down from (-1.25, -15) cm to (-1.3, -14) cm.

detected (see Fig. 9C). Then we switched the control of F2 from its tracking to the force modulating controller with a constant $e_{des,2} = \mu_2 e_{tr,2}$ with $\mu_2 = 0$. The experiment recorded signals are similar to those plotted in Fig. 5.

In this experiment, the cylindrical object was not fixed, but could move laterally under the influence of finger contact forces. Our results showed that we could achieve contacts between the fingers and object without moving the object. Then, once we applied $e_{des,i} = \mu_i e_{tr,i} > 0$, $\mu_i = 4$, $i = 1, 2$, i.e., we modulated forces, we were able to move the object. *This result shows that in principle, our approach is capable of manipulating a grasped object.*

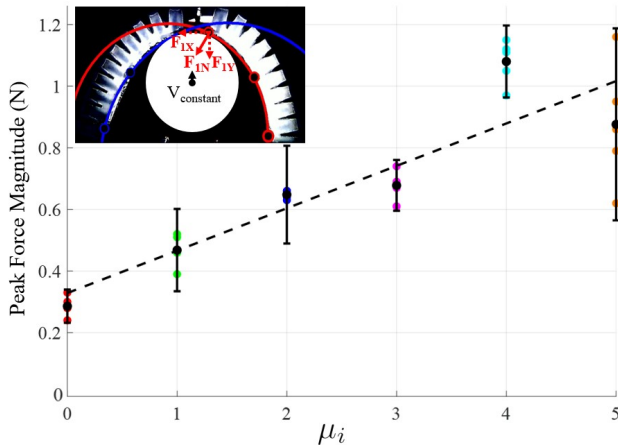


Fig. 10. The peak pull-out force during power grasping is plotted against the error values of the force controller for the cylinder with radius $r = 2$ cm and position at $(X_c, Y_c) = (0, 6.25)$ cm. Gentle power grasping can be achieved by setting $e_{des,i} = 0$ for a resulting pull-out force of ~ 0.3 N. The maximum pull-out force achieved is approximately ~ 1.2 N, with $e_{des,i} = \mu_i e_{tr,i}$, $\mu_i = 5$, $i = 1, 2$. The insert illustrates a free-body diagram of the measured force.

C. Modulation of Pull-Out Force

For the configuration of fingers and the object depicted in the insert of Fig. 10, we evaluate the pull-out force. We first apply the same sequence of references and control as in the previous experiments finishing with $\mu_1 = \mu_2 \in [0, 5]$, $e_{des,i} = \mu_i e_{tr,i}$. After the contact between the fingers and the object is stabilized, we initiate the motion of the cylindrical object in the $-Y$ direction and record the peak force exerted on the object. In this setup, the force sensor and the cylinder are mounted on a robot arm (Franka Robotics) which moves the cylinder at a constant velocity.

The plot of peak force magnitude vs. $\mu_1 = \mu_2$ values is shown in Fig. 10. As we can see, the peak force is consistently larger than two times the single finger force magnitude from Fig. 8. This is the result of the feedback control coping with keeping the errors $e_{f,i}$, $i = 1, 2$ small, i.e., keeping finger bending at the $y_{@con,i} + e_{des,i}$ values under the impact of the cylinder motion-induced displacement of the fingers. Although the values of used $\mu_1 = \mu_2$ do not offer a precise prediction of the peak pull-out force magnitude, they modulate the peak force through a roughly linear relation shown in the Fig. 10 plot.

VI. CONCLUSION

Our framework offers feedback control of the contact force of soft gripper fingers using kinesthetic (i.e., bending) sensing without the need for direct tactile or pressure sensors. The experiments show that the finger contact forces and their pull-out force are in a roughly linear relation with our control parameter, i.e., desired reference error. They also demonstrate that with our approach the controller can establish gentle contact with both fingers, irrespective of whether the object is symmetrically or asymmetrically positioned, and fixed or not. Furthermore, we show in Fig. 9 that we can modulate the force to move a grasped object.

Our approach should not only reduce the costs, but also enhance the reliability and ease of implementation of soft grippers. The sole requirement is the incorporation of any curvature or bending sensor. We used vision-based sensing, but any off-the-shelf stretchable bending sensors are also applicable. Potential applications of our approach include handling delicate objects, such as food, or harvesting fruits, where gentle force modulation is crucial.

In future work, we plan to implement our framework on a physical robotic arm equipped with soft dual-fingers, similar to [16]. Using reference signals, and feedback generated control and error variables, we will explore the use of machine learning for in-hand manipulation [17], and more adaptive and robust contact detection and grasping.

REFERENCES

- [1] S. Puhlmann, J. Harris, and O. Brock, "RBO hand 3: A platform for soft dexterous manipulation," *IEEE Transactions on Robotics*, vol. 38, no. 6, pp. 3434–3449, 2022.
- [2] S. Abundance, C. B. Teeple, and R. J. Wood, "A dexterous soft robotic hand for delicate in-hand manipulation," *IEEE Robotics and Automation Letters*, vol. 5, no. 4, pp. 5502–5509, 2020.

- [3] A. Pagoli, F. Chapelle, J. A. Corrales, Y. Mezouar, and Y. Lapusta, "A soft robotic gripper with an active palm and reconfigurable fingers for fully dexterous in-hand manipulation," *IEEE Robotics and Automation Letters*, vol. 6, no. 4, pp. 7706–7713, 2021.
- [4] L. Deng, Y. Shen, G. Fan, X. He, Z. Li, and Y. Yuan, "Design of a soft gripper with improved microfluidic tactile sensors for classification of deformable objects," *IEEE Robotics and Automation Letters*, vol. 7, no. 2, pp. 5607–5614, 2022.
- [5] Y. Luo, K. Wu, A. Spielberg, M. Foshey, D. Rus, T. Palacios, and W. Matusik, "Digital fabrication of pneumatic actuators with integrated sensing by machine knitting," in *Proceedings of the 2022 CHI Conference on Human Factors in Computing Systems*, 2022, pp. 1–13.
- [6] J. Qu, B. Mao, Z. Li, Y. Xu, K. Zhou, X. Cao, Q. Fan, M. Xu, B. Liang, H. Liu *et al.*, "Recent progress in advanced tactile sensing technologies for soft grippers," *Advanced Functional Materials*, p. 2306249, 2023.
- [7] P. Polygerinos, S. Lyne, Z. Wang, L. F. Nicolini, B. Mosadegh, G. M. Whitesides, and C. J. Walsh, "Towards a soft pneumatic glove for hand rehabilitation," in *2013 IEEE/RSJ International Conference on Intelligent Robots and Systems*, 2013, pp. 1512–1517.
- [8] M. Boivin, D. Milutinović, and M. Wehner, "Movement error based control for a firm touch of a soft somatosensitive actuator," in *2019 American Control Conference (ACC)*, 2019, pp. 7–12.
- [9] M. Boivin, K. Y. Lin, M. Wehner, and D. Milutinović, "Proprioceptive touch of a soft actuator containing an embedded intrinsically soft sensor using kinesthetic feedback," *Journal of Intelligent & Robotic Systems*, vol. 107, no. 28, pp. 1–18, 2023.
- [10] M. Boivin, C. Esch, M. Wehner, and D. Milutinović, "Feedback control for inflatable soft robotic finger touch detection based on static pressure-resistance characteristics," in *2023 American Control Conference (ACC)*, 2023, pp. 159–164.
- [11] M. Boivin, M. Wehner, and D. Milutinović, "Compliant proprioceptive touch without a force sensor: A kinesthetic feedback control approach," in *2022 IEEE Conference on Control Technology and Applications (CCTA)*, 2022, pp. 455–461.
- [12] R. S. Dahiya, G. Metta, M. Valle, and G. Sandini, "Tactile sensing—from humans to humanoids," *IEEE Transactions on Robotics*, vol. 26, no. 1, pp. 1–20, 2010.
- [13] S. Zou, S. Picella, J. de Vries, V. G. Kortman, A. Sakes, and J. T. B. Overvelde, "A retrofit sensing strategy for soft fluidic robots," *Nature Communications*, vol. 15, no. 539, 2024.
- [14] D. P. Holland, C. Abah, M. Velasco-Enriquez, M. Herman, G. J. Bennett, E. A. Vela, and C. J. Walsh, "The soft robotics toolkit: Strategies for overcoming obstacles to the wide dissemination of soft-robotic hardware," *IEEE Robotics & Automation Magazine*, vol. 24, no. 1, pp. 57–64, 2017.
- [15] C. Armanini, F. Boyer, A. T. Mathew, C. Duriez, and F. Renda, "Soft robots modeling: A structured overview," *IEEE Transactions on Robotics*, vol. 39, no. 3, pp. 1728–1748, 2023.
- [16] M. S. Li, T. M. Huh, C. R. Yahnker, and H. S. Stuart, "Resonant pneumatic tactile sensing for soft grippers," *IEEE Robotics and Automation Letters*, vol. 7, no. 4, pp. 10 105–10 111, 2022.
- [17] F. Khadivar and A. Billard, "Adaptive fingers coordination for robust grasp and in-hand manipulation under disturbances and unknown dynamics," *IEEE Transactions on Robotics*, vol. 39, no. 5, pp. 3350–3367, 2023.